Nanoscale

Accepted Manuscript

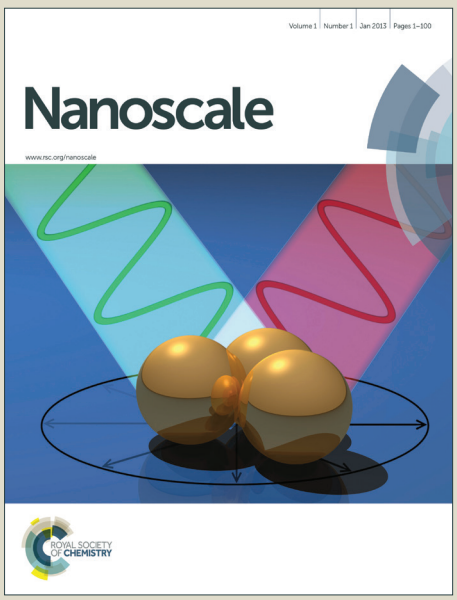

ROYAL SOCIETY OF CHEMISTRY

www.rsc.org/nanoscale

Journal Name
Nanoscale

Cite this: DOI: 10.1039/c0xx00000x

www.rsc.org/xxxxxx

ARTICLE TYPE

Luminomagnetic bifunctionality of Mn^{2+}-bonded graphene oxide /reduced graphene oxide two dimensional nanosheets

Amandeep Yadav[a,†],Garima Kedawat[b,†],Pawan Kumar[a], Avaneesh Anshul[a], Abhay D. Deshmukh[c], Om Pal Singh[a], R. K. Gupta[d], S. S. Amritphale[e], Govind[a],V. N. Singh[a] and Bipin Kumar Gupta[a,*]

Received (in XXX, XXX) XthXXXXXXXXX 20XX, Accepted Xth XXXXXXXXX 20XX
DOI: 10.1039/b000000x

Herein, we report the luminomagnetic bifunctional properties of two-dimensional (2D) Mn^{2+} bonded graphene oxide (GO)/reduced graphene oxide (RGO) nanosheets synthesized using a facile route of oxidation followed by solvothermal reduction method. Photoluminescence (PL) studies (excited by different wavelengths) revealed that the resonant energy transfer between Mn^{2+} and sp^3/sp^2 clusters of GO/RGO is responsible for the enhancement of emission. Moreover, the pH-sensitive PL behaviors have also been investigated in details. The ferromagnetic behavior is believed to arise due to defects in Mn^{2+} bonded GO composite. Thus, our reduction method provides a direct route to tune and enhance the optical properties of GO and RGO nanosheets bonded with Mn^{2+} ions, which creates an opportunity for various technological applications.

1. Introduction

Graphene with a honeycomb lattice has proven to be a new wonder material because of its applications in almost all branches of emerging science and technology.[1] Despite intense interest and extensive studies, achieving luminescence from zero band gap graphene is limited by its poor solubility. Graphene oxide (GO) is an atomically thin sheet of graphite which has traditionally served as a precursor for graphene. It is covalently decorated with oxygen and/or oxygen-containing functional groups at both the basal planes and edges.[2] It shows a good range of solubility in water and other oxygenic solvents, which allows it to be easily deposited onto a wide range of substrates.[3] Recently, luminescent GO has attracted research interest in optoelectronics and biological applications due to its tunable optical properties.[4-6] Reduced graphene oxide (RGO), characterized as an incompletely reduced product of GO, is an intermediate product between graphene and GO. The unique chemical structure of GO and RGO along with their heterogeneous electronic structures (due to the presence of sp^2 and sp^3 bonding) confer the exciting prospects for new applications. Both RGO and GO reveal a bandgap that can be tuned over a large range of energies, suggesting that the functionalization of graphene by oxidation can modify its optical, mechanical, electrical properties[7,8] and can also change the various photoluminescence (PL) features.[9]

The chemically functionalized GO and RGO exhibit a broad luminescence emission from ultraviolet to near infrared.[4,9] The PL emission of GO is a quasi-molecule fluorescence[10] and it is also affected by various factors such as pH value[11] and solvent[12] used for chemical reduction.[13] The fluorescence of GO over a wide range of wavelengths offers possibilities for incorporation into blue light-emitting diodes, white light emission for solid-state lighting and display applications on flexible platforms.[14] The low-energy fluorescence of GO or graphene quantum dots in red to near infrared (NIR) wavelengths is useful for biological applications.[16] In addition, mechanically exfoliated single-layer graphene has shown broad luminescence from 400 to 800 nm.[15] Red-to-near-infrared PL emitted from chemically-reduced GO is consistent with increasing disorder length scale with reduction.[16] The red emission in GO is due to a disorder-induced localized state related transition.[4] Moreover, the blue emission in GO is also reported from electron-hole recombination among sp^2 clusters enclosed by sp^3 defects.[17] The RGO and graphene quantum dots have also demonstrated blue fluorescence with a relatively narrow bandwidth.[17,18] The PL emission of GO can be tuned from red to blue by changing the amount of sp^2- and sp^3-bonded carbon atoms through the reduction oxygen containing functional groups at surface.[4] An excitation wavelength dependent PL with strong blue emission is achieved from graphene quantum dots, synthesized by cutting the preoxidized graphene sheets.[18] This blue luminescence may have originated from free zigzag sites of a carbene-like triplet ground state. The PL peak shifted to a slightly longer blue wavelength (with decreasing intensity), when the excitation wavelength was changed from 320 to 420 nm.

A further elucidation of the oxygen-related defects in graphene is important for exploring a new approach for tuning the energy band structure of graphene via defect engineering. In addition, the accessibility of graphene surface also provides a unique opportunity to support chemical impurities that can modify the electronic and optical properties of graphene. Metal oxides can be uniformly dispersed on the plane of graphene and the charge transfer at the interface of these hybrid materials can show a synergistic effect to induce properties that are different from those of each individual components.[19,21] Recently, chemically modified fluorescent GO with n-butylamine has shown PL emission in which maximum emission shifted towards the higher wavelength. The emission intensity decreased, when the excitation wavelength was varied from 350 to 470 nm.[22] The intensity of long-wavelength PL was very weak despite the large scale distribution of sp^2 clusters. Gan et. al. reported that MnO_2-decorated RGO demonstrated tunable and enhanced PL in a broad wavelength range (400 to 550 nm) due to the resonant energy transfer between Mn^{2+} and sp^2 clusters.[23] Li et. al. proposed an excitation-independent blue emission with two stationary PLE peaks around 330 nm and 450 nm, which were due to the transfer of mediated energy from Mn^{2+} ions to the sp^2 carbon clusters, yielding a intense long-wavelength PL emission.[24]

In addition to this, magnetism of carbon based materials (graphene and its derivatives) is of particular interest, as the light weight magnets could open up new ways to design adaptable and flexible information storage systems.[25] The potential application of carbon-based magnets is in spin electronics because graphene has an extraordinary carrier mobility and this provides a way to integrate spin and molecular electronics easily.[26] These materials are also paid attention in biophysical and chemical sciences; since the spin dependent part of the electronic wave-function can affected the chemical bonding pathway. It is well-known that the ideal graphene is intrinsically non-magnetic, due to de-localized π bonding network, which limits its applications in spintronic.[27] The spin orientation in GO has been introduced through topological defect, vacancies and doping of 3d and 4f elements.[28] The room temperature magnetism adds an extra degree of freedom in their potential functionalities and functional group attached to a graphene skeleton also provides a net higher magnetization.[29] Low temperature ferromagnetism was reported in GO.[30] The ferromagnetic ordering in GO and RGO (lower oxygen concentration, higher vacancies and disorder) persist at low temperature. As temperature increases, phonon scattering destroys the net magnetic moment of free and bonded radicals.[28] It is difficult to achieve long range coupling of localized spin (at higher temperature) due to delocalization of electrons. The room temperature ferromagnetism in GO for functional applications can be achieved by the introduction of impurities of high spin state transition metals.[31]

Herein, we demonstrate single-step facile routes for the rapid synthesis of bifunctional Mn^{2+} bonded GO and RGO hybrid materials with pronounced and tunable PL phenomenon in wider wavelength range. The synthesis was carried out using the modified Hummer's method combined with solvothermal reduction method. Mn^{2+} bonded GO and RGO afforded intimate bonding and synergetic coupling effects, leading to significantly higher PL in GO as compared to RGO. The enhancement of PL is induced by Mn^{2+} mediated energy transfer process which is identified by the long decay lifetime. The X-ray photo spectroscopy revealed the covalent coupling of Mn^{2+} with GO/RGO, suggesting that these hybrid materials offer a promising strategy for advanced optoelectronics and bio-medical devices. To the best of our knowledge, this is the first report describing the bifunctional Mn^{2+} bonded GO and RGO hybrid materials for PL and magnetic properties. A detailed explanation of the origin of variable energy PL in Mn^{2+} bonded GO and RGO hybrid composite and the effect of pH on the optical properties have been presented in details and we also reported the room-temperature ferromagnetism in GO which provides guideline for the design of more subtle magnetic carbon devices.

2. Experimental

2.1 Synthesis of Mn^{2+} bonded graphene oxide and Mn^{2+} bonded reduced graphene oxide 2D nanosheets composite

The Mn^{2+} bonded graphene oxide and Mn^{2+} bonded reduced graphene oxide 2D nanosheets composite were synthesized using facile and inexpensive technique. Initially, GO was prepared using natural graphite powders by the Hummer's method.[32] The GO water suspension (100 mL, 0.5 mg/mL) with 0.0079 g of $KMnO_4$ powders was first ultrasonicated for 1 hr and then stirred for 15 mins. The obtained solution was kept in an oven at 60°C for 3 hrs and was cooled to room temperature. After carefully filtering and washing with de-ionized water and alcohol, the intermediate product was then dispersed in de-ionized water. 30 mL of the supernatant was poured into round bottom flask and heated at 200°C for 12 hrs. The black precipitate was dispersed ultrasonically in de-ionized water and the suspension was further dialyzed in a dialysis bag overnight at a temperature of ~4°C. The as-synthesized MnO_2 decorated GO product is obtained as an intermediated product in which MnO_4 is converted into MnO_2. Further, for Mn^{2+} complexation with GO and RGO lattice, we added COOH (10 mL) in intermediate product. This carboxyl group is reacted with MnO_2 nanoparticles in the presence of heated H_2O. Then, this functional group is removed after reaction and meanwhile, Mn^{2+} ions are bonded/complexation with available oxygen functionality in the GO and RGO lattice. It is also confirmed by spectroscopy technique as well as in high resolution microscopy as a metal contrast image of Mn cluster in graphene lattice. Similar observations have been previously reported for Eu, Pt or Au atoms on the graphene lattice or carbon nanotubes.[33,34] The pH was controlled by adding aqueous solution of NaOH drop-wise into the solution and simultaneously measuring the pH using pH meter. The effect of pH on the optical properties has been studied in detail. Henceforth, the Mn^{2+} bonded GO (MnGO) and Mn^{2+} bonded RGO (MnRGO) two dimensional (2D) nanosheet composite samples prepared at different pH values (4, 7 and 10)

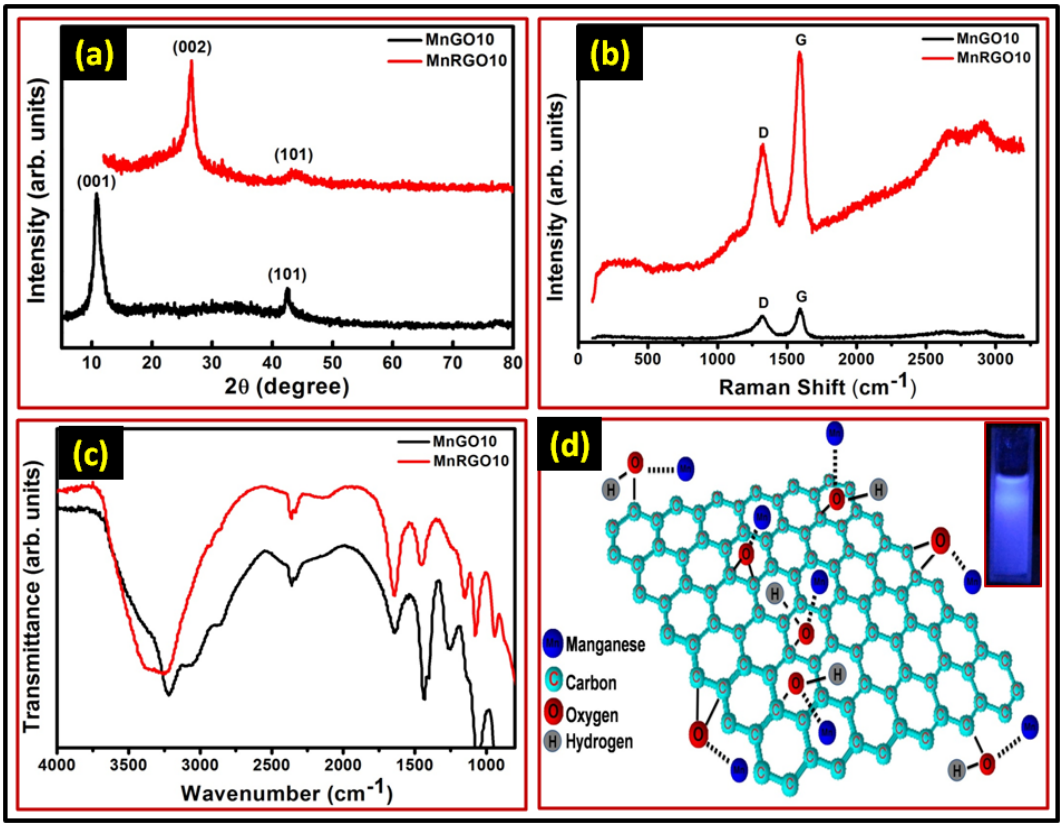

Fig. 1:(a) XRD spectra of MnGO10 and MnRGO10 composites, (b) Raman spectra of MnGO10 and MnRGO10 composites, (c) FTIR spectra of MnGO10 and MnRGO10 composites and (d) the plausible schematic model for MnGO10 composite, represents the bonding of the Mn^{2+} to the GO nanosheets lattices, inset shows the optical photograph of the MnGO10 composite suspension in a cuvette excited by wavelengths of 310 nm portable UV lamp, showing the blue emission is largely enhanced.

will be designated as; for Mn^{2+} bonded GO nanosheet composite (MnGO4, MnGO7, and MnGO10) and as for Mn^{2+} bonded RGO nanosheet composite (MnGO4, MnGO7, and MnGO10), respectively.

2.2 Characterization

X-ray diffraction studies of the powder samples have been carried out using Rigaku, Miniflex, CuKα; λ=1.5405 Å). Prior to the XRD measurement, the diffractometer was calibrated using silicon powder as reference material (d_{111}=3.1353Å).[35] The accurate lattice parameters were also obtained through a least square fitting method using computer-based unit cell refinement software.[36] Raman studies were carried out using an argon ion laser with a wavelength of 514.5 nm as the excitation source (Model Innova 70, Coherent). FTIR spectroscopic measurements were performed on a Thermo Scientific FTIR spectrometer (model: NICOLET 6700). Spectra were collected at a resolution of 2 cm^{-1} and each spectrum was an average of 32 scans. The XPS analysis was performed in an ultra-high vacuum (UHV) chamber equipped with a hemispherical electron energy analyzer (Perkin Elmer, PHI1257) using non-monochromatized Al Kα source (excitation energy of 1486.7 eV) with a base pressure of 4 x10^{-10} torr at room temperature. The surface morphology and micro-structural characterization were carried out by scanning electron microscopy (SEM, Model No. EVO MA 10 VPSEM) and high resolution transmission electron microscopy (HRTEM, Model No. Technai G20-twin, 200kv with super twin lenses having point and line resolution of 0.144 nm and 0.232 nm, respectively) equipped with energy dispersive x-ray analysis (EDAX) facilities for elemental studies. The chemical composition of MnGO10 nanosheet composite was analyzed by electron energy-loss spectrometer (EELS) using a spectrometer attached to the transmission electron microscope. UV-visible spectra were collected using a high resolution UV-Vis spectrophotometer (MODEL No.LS 55). The Photoluminescence (PL) characterizations were performed using photoluminescence spectrometer (Edinburgh FLSP-920) equipped with a xenon lamp as an excitation source. The time resolved PL (TRPL) spectroscopy measurements were recorded using an Edinburgh luminescence spectrometer (F900) equipped with a microsecond xenon flash lamp as the source of excitation. Magnetic measurement has been performed to investigate the magnetic properties of Mn bonded GO nanosheets using SQUID-VSM (SVSM, Quantum Design Inc. USA) instrument.

3. Results and discussion

To analysis the crystalline structure of as-synthesized samples, XRD studies were carried out. The XRD patterns of MnGO10 and MnRGO10 composites are shown in Fig. 1a.The most intense diffraction peak of GO (black curve) at ~10.4° with larger d-spacing (d= 0.865 nm) corresponds to the (001) reflection, which is characteristic of stacked GO sheets. The interlayer spacing, d of GO is significantly larger compared to that of 0.34 nm for pristine graphite due to the attachment of oxygen-containing functional groups on both sides of graphene sheet.[37] Thus, from the XRD pattern of MnGO10, it could be revealed that the original graphite powders has almost been completely oxidized. The XRD pattern of MnRGO10 composite (RGO is exfoliated into individual platelets by the chemical reduction of GO) shows a very broad reflection at ~23.1° as shown in Fig. 1a (red curve). The shift of the characteristic diffraction peak of graphite from 26.58° to 23.1° is due to presence of short-range order in the stacked stacks. The interlayer spacing of RGO was 0.345 nm, which is slightly larger than that of graphite, due to the presence of small amount of residual oxygen-containing functional groups or other structural defects.[38] The particle size of MnGO10 and MnRGO10 composite is estimated by Schemer's formula. The average sheet size of MnGO10 and MnRGO10 composite is found to be 150 and 300 nm, respectively. Besides these representative diffraction peaks of GO and RGO, no other peaks belonging to Mn is detected in the XRD patterns. This is ascribed to the low amount of Mn in the composite samples uniformly dispersed and encapsulated in GO and RGO nanosheets (instead of being agglomerated) as revealed by microscopic observations.

Raman spectroscopy is considered to be a very convenient and nonvolatile technique for the information about the structure of the graphene sheets and its composite. The structural changes occurring during the chemical processing (from GO to RGO nanosheets) have been characterized using Raman spectroscopy. The Raman spectral profile for MnGO10 (black curve) and MnRGO10 (red curve) composites is shown in Fig. 1b. The Raman spectra displayed two remarkable peaks at 1350 and 1580 cm^{-1}, corresponding to the well documented D and G band, respectively. Here, the D band is associated with the structural defects and disorder carbon in the graphitic layers, whereas the G band corresponds to the E_{2g} mode of sp^2-hybridized C–C bonds in a two-dimensional hexagonal lattice.[39] The intensity of two peaks depends on the sp^2/sp^3 ratio.[40] Moreover, the relative strength of D band compared to G band usually signifies higher degree of disorderness related to exfoliation and extent of defects in the graphitic materials.[41] The size of the sp^2 domains increases during reduction of GO.[42] As shown in Fig. 1b, the I_D/I_G ratio gets reduced slightly from ~1.01 for MnRGO10 composite to ~0.92 for MnGO10 composite, due to the decrease in the average size of in-plane sp^2 domains, an increase of the edge planes, as well as the expansion of the disorder during the reduction of exfoliated GO, indicating the conversion of GO into RGO nanosheets.[43] There are no peaks corresponding to Mn or its compound in the Raman spectra of MnGO10 and MnRGO10 composite, which is consistent with the XRD data. The FTIR spectral measurements have been used for further confirmation of the reduction of oxygen containing functional groups of GO and to investigate the bonding composition of as-synthesized samples. Fig. 1c shows the FTIR spectra of MnGO10 (black curve) and MnRGO10 (red curve) composite samples. The FTIR spectrum of MnGO10 shows the presence of different types of oxygen functionalities in GO; such as, oxygen stretching vibration (3370 cm^{-1}, -OH vibration), C=O stretching vibration (1720 cm^{-1}), C-OH stretching vibration (1500 cm^{-1}), and C-O stretching vibration (1460 cm^{-1}). Importantly, the recorded FTIR spectrum clearly shows the presence of oxygen containing functional groups and also confirms that oxygen groups has not been removed from the graphene basal plane. Moreover, the signature of aromatic C=C stretching vibration of graphitic domains at ~1600 cm^{-1} indicates the presence of sp^2 hybridized honeycomb lattice. In the case of MnRGO10 composite spectrum, few modes are suppressed because of the reduction of GO into RGO. This implies that most of the carboxyl groups have been removed by the solvothermal treatment. Based on the above results, a schematic model of proposed bonding of the Mn^{2+} to the GO nanosheets lattices is shown in Fig. 1d. The inset of Fig. 1d displays the optical photograph image of MnGO10 suspension kept in a cuvette and excited by 310 nm portable UV lamp. The optical photo was taken by Nikon high-resolution digital camera and it reveals that the blue emission is largely enhanced.

The morphologies of Mn^{2+} bonded GO/RGO composite samples were investigated using SEM and TEM. Fig. 2a shows the SEM image of free-standing MnGO10 nanosheet composite; consisting of crumpled and rippled structure closely associated to each other, which might be attributed to the defective structure formed due to the exfoliation and restacking processes. The MnRGO10 nanosheets composite, however, are layer structured, irregular and folded, as shown in the SEM image of Fig. 2b and 2c. Fig. 2c is high-magnification view of Fig. 2b. These nanosheets are entangled with each other. The SEM images revealed that the dimension of MnGO10 and MnRGO10 nanosheets are about 150 and 300 nm, respectively. The dark contrast embedded on layers shows the presence of MnO_2 particles on the graphene sheets (Fig. 2a and 2c), which is further confirmed by TEM/HRTEM studies. It can be seen that MnO_2 decorates the surface of GO/RGO nanosheets and the folding and wrinkling characters of graphene sheets are well preserved. As shown in Fig. 2d and 2e, (TEM observation of MnGO10 nanosheets) MnO_2 is well bonded to the GO nanosheets. Fig. 2g and 2h show the TEM images of single- or few-layered MnRGO10 nanosheets, which are transparent and have lots of wrinkles. Corrugation and scrolling suggest the intrinsic nature of graphene. The existence of 2D graphene sheets is shown with an arrow in Fig. 2e and 2h. The Mn^{2+} ions bonded over the few layers of graphene sheet is clearly seen as black dots in the image (Fig. 2e and 2h). Through the first-principles calculations, it has been shown that 3d-transition metal atoms have a covalent bonding with graphene due to the hybridization between the $d_{x^2-y^2}$ and d_{yz} orbitals of the metal atoms and p_z orbitals of the carbon atoms. The high affinity of these metal atoms to the non-perfect and strained regions of graphene sheets allows one to bind the

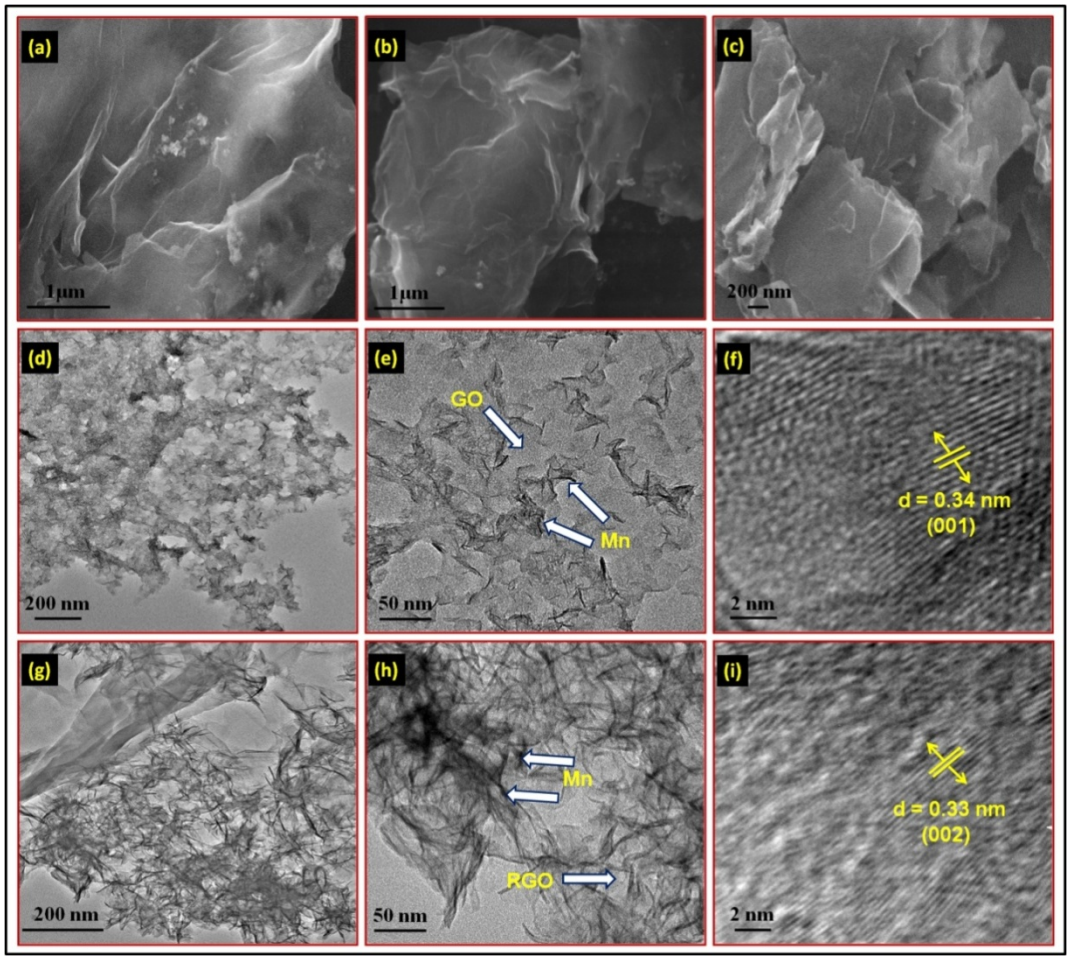

Fig. 2: (a) SEM image of MnGO10 nanosheet composite, (b) SEM image of MnRGO10nanosheet composite, (c) magnified view of Fig. 2b, (d) TEM image of MnGO10 nanosheet composite, (e) magnified view of Fig. 2d; arrows represent the presence of MnO_2 particles on 2D graphene oxide nanosheets with black dotted structure and graphene oxide nanosheets, (f) HRTEM image of MnGO10 nanosheet composite, (g) TEM image of MnRGO10 nanosheet composite, (h) magnified view of Fig. 2g; arrows represent the presence of MnO_2 particles on 2D reduced graphene oxide nanosheets with black dotted structure and reduced graphene oxide nanosheets and (i) HRTEM image of MnRGO10 nanosheet composite.

metal atoms to the graphene, and these in effect tailor the properties of graphene or carbon based materials. Thus, the bonding of MnO_2 particles to the GO/RGO nanosheets significantly transfer the efficient energy. The high-resolution TEM images of MnGO10 and MnRGO10 composite (Fig. 2f and 2i) show the lattice fringes with d spacing of ~0.34 nm and ~0.33 nm, corresponding to the (001) and (002) plane of GO and RGO, respectively, which are consistent with the XRD pattern. This is further confirmed by the presence of Mn^{2+} ions bonded to the GO and RGO nanosheets as shown through the XPS studies. The cluster size of Mn (>1 nm) in Mn^{2+}-bonded in graphene lattice can be realized from metal cluster contrast images from the Fig. 2f and 2i.

To understand the composition and chemical nature of MnGO10 and MnRGO10 composite samples, the XPS measurements have been performed (Fig. S1; see Supporting Information). The XPS survey spectra of MnGO10 and MnRGO10 composite are shown in Fig. S1a and S1c, respectively, indicating the presence of carbon, oxygen and Mn elements. No other element was detected. These results further confirmed the insufficient reduction of GO by chemical reduction method, which is consistent with results of XRD. The high resolution spectra of C1s region for MnGO10 and MnRGO10 composite are shown in Fig. S1b and S1d, respectively. The differences between the C1s spectra of MnGO10 and MnRGO10 are evident from the shape and peak identity. XPS analysis demonstrated that the main peak positioned at about 284.6 eV is due to non-oxygenated carbon atoms ring (sp^2 C-C bond), while the other peaks at 286.7, 287.8 and 289.1 eV correspond to the oxygen containing groups (C–OH), (C = O) and (O = C–OH), respectively (Fig. S1b). However, according to C1s spectra analysis of MnRGO10 in Fig. S1d, after the chemical reduction of GO, the intensity of characteristic peaks for the oxygen containing functional groups significantly decreased, though not

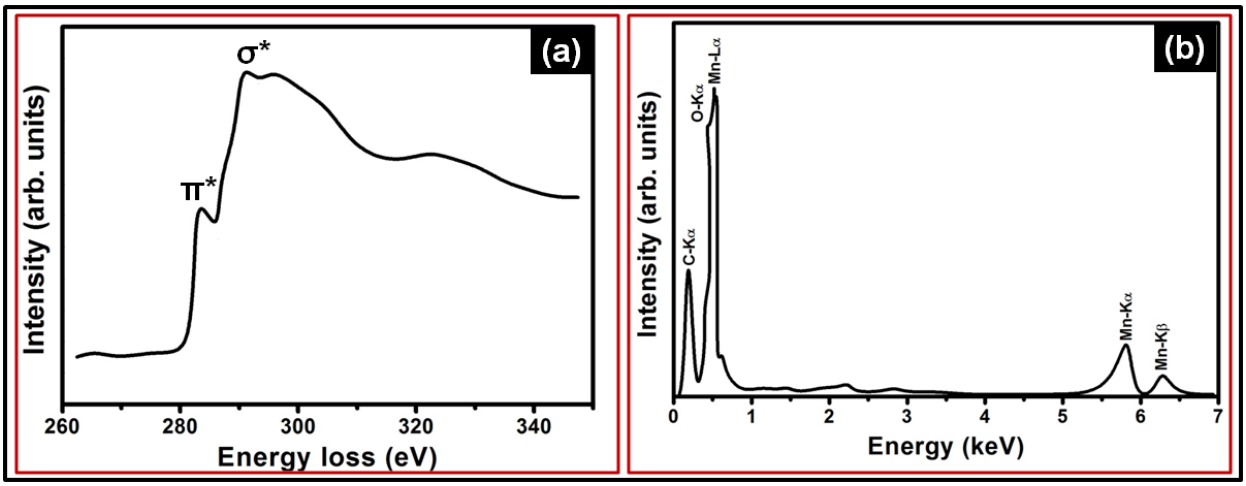

Fig. 3: (a) EELS and (b) EDX spectra of MnGO10 nanosheet composite.

completely vanished, which are in good agreement with FTIR results. A significantly larger proportion of oxygen in GO existed in the form of C-O functionalities and fewer proportion of oxygen are associated with hydroxyl and O-C=O groups. The peaks of oxygen-containing groups at 284.5 eV (C-O), 286.8 eV (C=O), and 289 eV (O-C=O) decreased to different degrees. The proportion of C=O group decreased greatly and O-C=O group vanished, while the proportion of hydroxyl groups changed slightly, demonstrating that chemical reduction method has little effect on the deoxygenation of hydroxyl groups. The core level peak of O1s for MnGO10 composite is shown in Fig. S1e, peaking at 532.1 eV binding energy. The Mn2p XPS spectra acquired from the synthesized composite product confirmed the existence of Mn oxide. The high resolution core level peaks of Mn2p for MnGO10 and MnRGO10 composite are shown in Fig. S1f and S1g, respectively. Only single peak appeared at ~641.3 eV corresponding to Mn $2p_{3/2}$ and two symmetrical peaks at ~641.6 eV and ~656 eV corresponding to Mn $2p_{3/2}$ and Mn $2p_{1/2}$ for MnGO10 and MnRGO10 composites, respectively are presented. The spin orbit splitting between Mn $2p_{3/2}$ and Mn $2p_{1/2}$ is ~14.4 eV, suggesting the formation of MnO_2 and corresponds to the 2p binding energy of Mn^{2+} ions. The oxidation properties of manganese, Mn 2p peaks position and solubility of Mn ions in acid alkali solutions indicate that at all mentioned pH values, Mn^{2+} ions remain bonded to the surface of all as-synthesized composites related to GO and RGO nanosheets. Furthermore, electron energy loss spectroscopy (EELS), and energy dispersive X-ray spectroscopy (EDX) were used to study the elemental analysis, structure and chemistry of the as-prepared composite samples. The EELS and EDX spectra of MnGO10 nanosheet composite are shown in Fig 3a and 3b. It indicates the presence of C, O and Mn elements in the as-synthesized composite as well as formation of Mn^{2+} ions complex in honeycomb carbon lattice.

The UV–vis absorption spectra of MnGO10 and MnRGO10 composite dispersed in water is shown in Fig. 4a. As can be seen from Fig. 4a, the absorption peak of MnGO10 is in the range of 231 to 270 nm. A typical absorption peak at approximately 250 nm arises due to the π-π* transition of C-C and C=C bonds in sp^2 hybrid domain regions, and a shoulder peak observed at approximately 300 nm is due to the π-π* transition of the C=O bond in sp^3 hybrid regions. Whereas, the absorption peak of RGO is shifted towards the blue wavelength region, which may be attributed to the exfoliation of layered GO sheets during the synthesis process.[12,44]

To explore the optical properties of MnGO10 and MnRGO10 composite samples, a detailed PL study was carried out at room temperature. The new interesting enhanced PL behavior is observed in as-synthesized MnGO10 and MnRGO10 composite. It is well known that, the intrinsic and tunable fluorescence from GO or RGO could open exciting and previously unforeseen optical applications for graphene-based materials. The strongly heterogeneous atomic and electronic structures of GO indicate that fluorescence in GO arises from recombination of electron-hole pairs in localized electronic states originating from various possible configurations, rather than from band-edge transitions similar to the case of typical semiconductors. In order to understand the wavelength dependence and the excitation wavelength at which PL intensity is maximum, the PL emission and excitation spectra for MnGO10 and MnRGO10 composite are carried out and the results are shown in Fig. S2 (see supporting information). An enhanced and tunable PL in the visible range is observed. The various PL emission spectra for MnGO10 composite were recorded at different excitation wavelengths ranging from 250 to 500 nm (Fig. S2a). The PL peak position shifts towards longer wavelength side by varying the excitation wavelength. A strong blue emission is obtained at 410 nm, when the sample is excited with 300 nm wavelength. It has been reported that isolated sp^2 clusters within the carbon-oxygen sp^3 matrix could yield band gaps consistent with blue emission due to the localization of electron-hole pairs.[17] The PLE spectra for MnGO10 composite at different emission wavelength from 357 to 488 nm are shown in Fig. S2b. It is observed that at 418

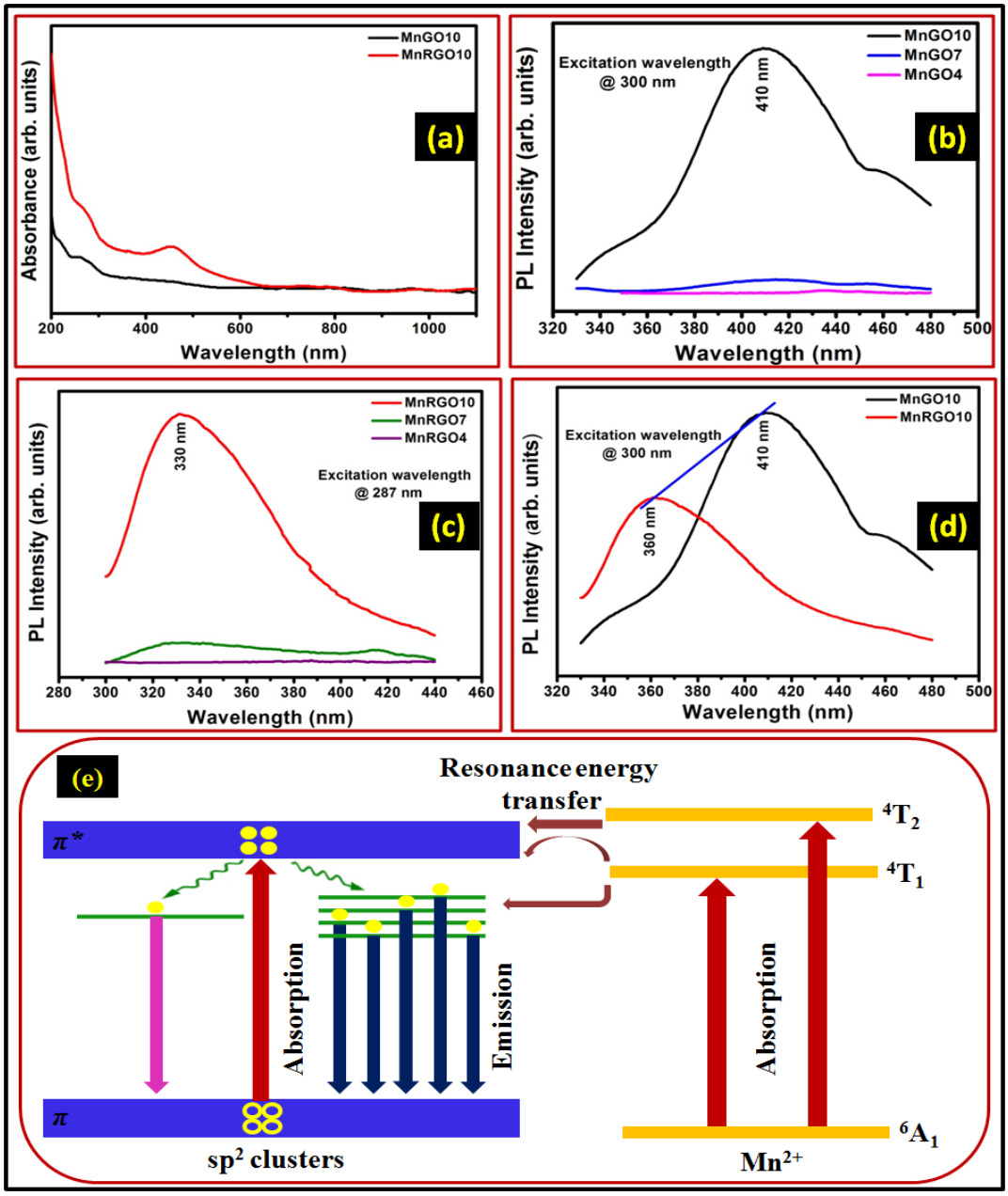

Fig. 4: (a) UV–vis absorption spectra of MnGO10 and MnRGO10 composite, pH dependence PL spectra for (b) MnGO, (c) MnRGO composite having different pH values (4, 7 and 10), (d) dependence of PL blue-shift of the MnRGO10 composite sample compared to MnGO10 composite (represented by solid blue line) on the value of sp^2 fraction and (e) plausible schematic mechanism energy-level diagram of MnGO10 composite explaining the PL emission in GO associated with the Mn^{2+} mediated energy transfer process; the blue emission is attributed at 410 nm wavelength due to the $^4T_2$ to $^6A_1$ transition of Mn^{2+}. The energy transfer from Mn^{2+} to sp^2 clusters corresponds to variable and broad PL emission.

nm emission wavelength, the excitation is maximum at 315 nm wavelength.

Similarly, the corresponding PL and PLE spectra for MnRGO10 composite are displayed in Fig. S2c and S2d, respectively. The emission wavelength remains centered at about 330 nm, when the excitation wavelength is varied from 250 to 290 nm and the PL intensity also varies depending on the excitation wavelength (Fig. S2c). When the excitation wavelength was increased from 310 nm to higher values, the emission spectra shifted towards longer wavelength region. The red shift observed in the PL spectra (with increasing excitation wavelengths) is essentially a quantum confinement effect related to the size of the sp^2 clusters. When the sample is excited by 287

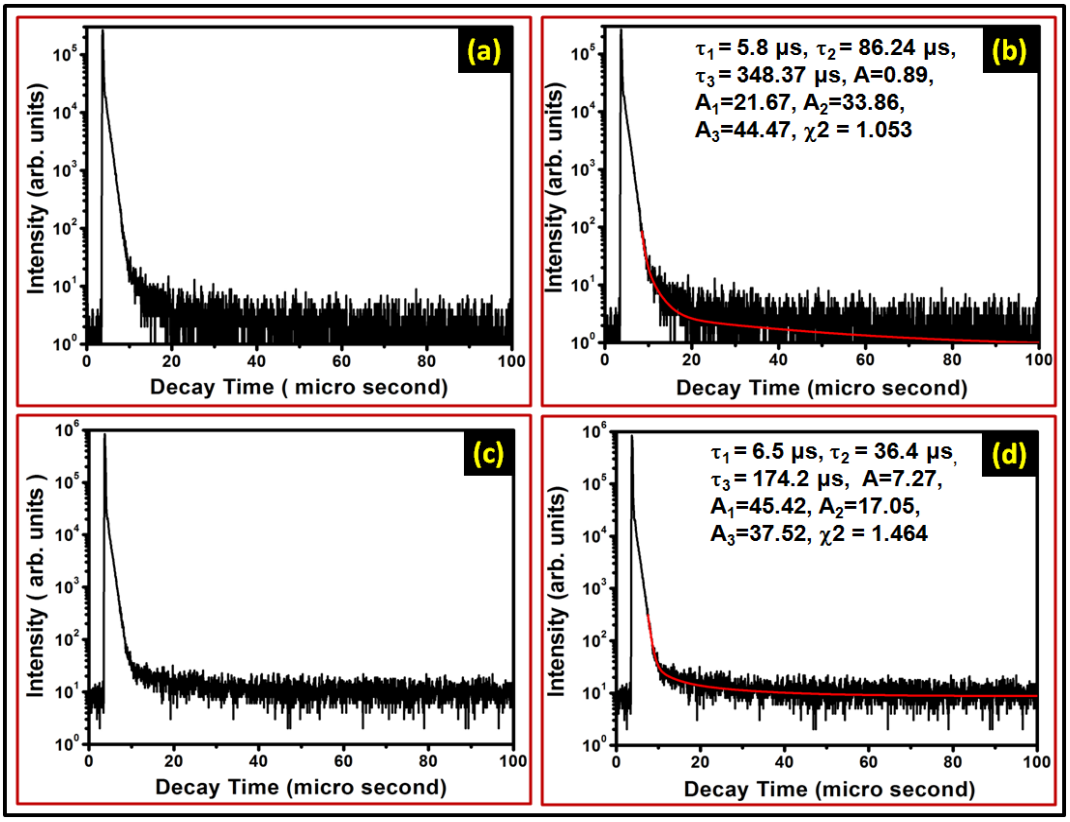

Fig. 5: (a) Time resolved PL decay profile of MnGO10 composite recorded at room temperature, (b) the exponential fitting curve of MnGO10 composite with lifetime data parameters generated by exponential fitting, (c) time resolved PL decay profile of MnRGO10 composite recorded at room temperature and (d) the exponential fitting curve of MnRGO10 compositewith lifetime data parameters generated by exponential fitting.

nm, a broad emission with maximum intense peak at 330 nm is observed. In addition, the PLE spectra of MnRGO10 composite at different emission wavelength from 300 to 620 nm are also shown in Fig. S2d. It is observed that at 332 nm emission wavelength, a broad peak is obtained at 287 nm. At higher emission wavelength from 395 to 620 nm, PL intensity gets suppressed to a greater extent. The excitation wavelength dependence of the emission wavelength and intensity is a common phenomenon observed in carbon-based materials. The predominant broad emission band in the as-synthesized MnGO and MnRGO composite samples for a wide-range of excitation energies may be attributed to optical transitions from these disorder-induced localized states, emissive traps, electronic conjugate structures, and free zigzag sites.

The proposed PL mechanism based on the emissive free zigzag sites is further supported by the observed pH-dependent PL. The PL emission spectra of the MnGO composite with different pH values 4, 7 and 10 are shown in Fig. 4b. The PL emission of MnGO composite is very sensitive to pH value, having better fluorescence at higher pH value and the emission wavelength does not shift with increase of pH value. For MnGO10, under an excitation wavelength of 300 nm, high peak intensity is observed at near-UV wavelength of 410 nm. It is well known that the blue PL originates from localized sp^2 domains within sp^3 matrix.[17] The PL emission spectra for MnRGO composite at different pH values (4, 7 and 10) are shown in Fig. 4c. As can be seen in Figure, under excitation wavelength 287 nm, a broad band emission is observed at 330 nm. The fluorescence of carbon based material is pH dependent. At higher pH values, the fluorescence is strong enough that it can be observed even by naked eye, whereas it is nearly quenched at lower pH conditions. MnGO and MnRGO composites at different low pH values showed drastic suppression of the PL signal, which may be ascribed to the protonation of the emissive zigzag sites with $\sigma^1\pi^1$ ground state in acidic conditions which quenches the fluorescence, whereas de-protonation in alkaline conditions recovers it. Thus, under alkaline conditions, the MnGO and MnRGO composite emit strong PL, whereas, under acidic conditions, the PL is nearly quenched. When pH is varied between 4 and 10, the PL intensity increases rapidly. The PLE spectra for MnGO and MnRGO composite at different pH values (4, 7 and 10) are also shown in Fig. S3a and Fig. S3b (see supporting information), respectively. Fig. 4d displays the PL emission spectra of MnGO10 and MnRGO10 composite. Strong PL emission from MnGO10 and weak PL emission from MnRGO10 have been observed under the excitation by 300 nm laser light. For the MnGO10, the broad band emission in the 330-480 nm (short wavelength range) is observed and the main feature shifts toward shorter wavelength (from 410 nm for

MnGO10 to 360 nm for MnRGO10 composite). The emission peak position and width depends on the sp^2 fraction. Interestingly, the PL blue-shift is due to reduction of functional group in MnRGO10 composite, as indicated by the solid blue line in Fig. 4d. It suggests that the increase in sp^2 fraction may be responsible for the PL blue-shift of MnRGO10 composite and one can tailor the PL blue-shift by tuning the sp^2 fraction of the MnRGO10 composite samples. The PL of MnRGO10 composite shows the maximum blue-shift of approximately 50 nm. It can be noticed that in the case of graphene oxide having pH10 (MnGO10), the intensity of emission and excitation spectra get enhanced compared to other samples. It may be due to efficient energy conversion from oxygen functionality to Mn^{2+} in compared to RGO lattice.

The plausible schematic mechanism explaining the PL from MnGO10 composite is illustrated in Fig. 4e. It is well known that (i) the optoelectronic properties of carbon based materials are mainly determined by the π and π* states of the sp^2 sites which lie within the σ – σ* gap and (ii) the PL emission of GO mainly originates from sp^2 clusters that are isolated within the sp^3 carbon-oxygen or defects. The RGO have a higher content of oxygen functional groups, suggesting that it consist of numerous disorder-induced defect states within the π– π* gap.[23] It was proposed that (i) π bonding is weaker and has lower formation energy than σ bonding; and (ii) a large number of disorder-induced localized states are in the two-dimensional network of RGO composite, which consists of a large fraction of distorted carbon atoms attached to oxygen-containing functional groups. After the reduction of GO into RGO, the number of disorder-induced states within the π – π* gap decreases, and an increased number of cluster-like states from the newly formed isolated sp^2 domains are formed. Therefore, the electron-hole recombination among these sp^2 cluster-like states with variable bandgap corresponds to the excitation-dependent emission by GO and RGO composites.

The variable PL emission for different excitation wavelength for MnGO and MnRGO composite is due to the disorder-induced localized defect states at carbenelike zigzag sites. The introduction of Mn^{2+} ions are also associated with the mediated emission in GO and RGO composite, which corresponds to the $^4T_2$ to $^6A_1$ transition of Mn^{2+}. Since Mn^{2+} is bonded to the sp^2 clusters, the short distance and energy level overlap lead to effective energy transfer from Mn^{2+} to the sp^2 clusters. As a result, the radiative recombination rate increased significantly and the PL spectra consequently enhanced. When the excitation wavelength was shorter than 400 nm, the $^6A_1$ to $^4T_2$ mediated transition state of Mn^{2+} is gradually dominantly get excited and the energy is transferred quickly to the sp^2 clusters in GO, resulting in the blue PL emission at 410 nm for MnGO composite. The emission by the synthesized composites occurs due to the presence of a large scale of sp^2 clusters and resonant energy transfer between Mn^{2+} and sp^2 clusters due to pH-dependent reversible solubility of Mn^{2+}-related salts. Additionally, the broad PL emission at ~410 nm for MnGO composite is attributed to the light absorption by the broad energy gap of the sp^2 clusters. Hence, the presence of the $^4T_2$ level of Mn^{2+} also causes the excited electrons to occupy the energy level situation at 300 nm energy level. These electrons relax non-radiatively to the next lower level centered at 410 nm and radiative recombination occurs. The enhanced and broad PL peak centered at 410 nm can thus be mainly attributed to the introduction of Mn^{2+}. When the excitation wavelength is longer than 400 nm is used, lower energy photons cannot be absorbed by Mn^{2+}, therefore, the PL intensity diminished. The presence of Mn^{2+} energy levels causes effective absorption by few sp^2 clusters with low energy levels. The radiative recombination to the ground state, together with the process of transfer between Mn^{2+} and sp^2 clusters, produces the enhanced PL. Since the transition probability of $^4T_2$ to $^6A_1$ from Mn^{2+} is much higher than that of $^4T_1$ to $^6A_1$, the 410 nm emission is the most intense. Moreover, the MnRGO composite may exhibit purple PL at shorter wavelengths. In other words, reduction may increase the number of small sp^2 domains, resulting in the PL spectra of MnRGO composite shifting from blue to shorter wavelength.

The decay lifetime is an important parameter to investigate the emission mechanism as well as for deciding the performance of materials for their suitable use. The efficiency of radiative recombination is directly proportional to the decay time of the particular transition. The luminescence decay curve of MnGO10 and MnRGO10 composite is shown in Fig. 5. It was measured at room temperature by a time-correlated single photon counting spectrometer with a picosecond diode laser of 375 nm as source of excitation. The lifetime data obtained for MnGO and MnRGO composite were fitted to a triple-exponential function as,[45-47]

$$I(t) = A_1\exp(-t/\tau_1)+A_2\exp(-t/\tau_2)+A_2\exp(-t/\tau_3) \quad (1)$$

Where τ_1, τ_2 and τ_3 are the decay lifetimes of the luminescence, and A_1, A_2 and A_3 are the weighting parameters. The radiative transition is observed at 410 nm with 300 nm excitation for MnGO10 composite and the decay profile is shown in Fig. 5a. The Fig. 5b demonstrates the exponential fitting of decay profile, as described in equation (1) and the corresponding parameters generated from fitting are listed in the inset of Fig. 5b. The observed lifetimes are $\tau_1 \sim 5.8$ μs, $\tau_2 \sim 86.24$ μs and $\tau_3 \sim 348.37$ μs. The average lifetime for MnGO10 composite is $\tau_{av} \sim 304$ μs. The radiative transition is observed at 330 nm with 287 nm excitation for MnRGO10 composite and the decay profile is shown in Fig. 5c. Fig. 5d demonstrates the exponential fitting of decay profile, as described in equation (1) and the corresponding parameters generated from fitting are listed in the inset of Fig. 5d. The observed lifetimes are $\tau_1 \sim 6.5$ μs, $\tau_2 \sim 36.4$ μs and $\tau_3 \sim 174.2$ μs. The average lifetime forMnRGO10 composite is $\tau_{av} \sim 156$ μs. It should be noted that the PL decay lifetime in MnGO10 is rather faster compared to MnRGO10 and the decay lifetime is of the order of microseconds. This long lifetime indicates the involvement of some extra charge carrier transport or recombination. Based on these observations, we proposed that

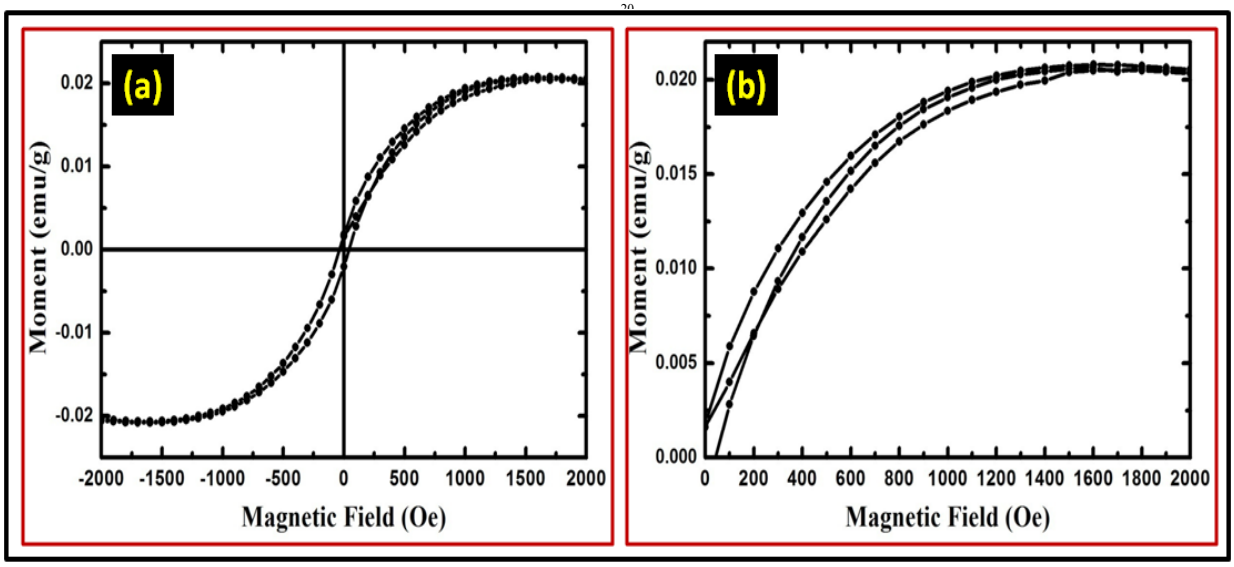

Fig. 6: (a) Magnetization hysteresis loop at room temperature in the range of -2 kOe ≤ H ≤ +2kOe for MnGO10 composite and (b) magnified view of Fig. 6a in the positive quadrant of magnetic field (from 0 kOe≤ H ≤ +2 kOe).

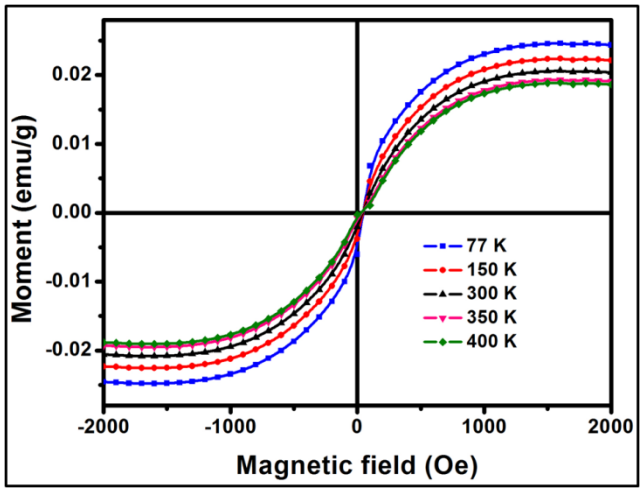

Fig. 7: Isothermal magnetization (M-H) observed on MnGO10 composite collected from H of -2 kOe to +2kOe at various temperatures 77, 150, 300, 350 and 400 K.

Mn^{2+} acts as an intermediate state in the carrier decay process, which can well explain the observed long decay lifetime. The PL emission wavelength shift towards shorter wavelength (Fig. 4d). The intensity of PL peak (MnGO) is higher than the peak of MnRGO composite. This longer emission wavelength exhibits relatively longer carrier lifetime.

The magnetization hysteresis loops at room temperature in the range of -2kOe ≤ H ≤ +2kOe for MnGO10 composite is shown in Fig. 6a and its magnified view (the positive region of magnetic field from 0 kOe ≤ H ≤ +2 kOe) is depicted in Fig. 6b. The as-synthesized MnGO10 composite sample show weak ferromagnetism with saturation magnetization M_s = 0.020 emu/g at room temperature. The magnetization gets saturated at 1800 Oe for the sample. It is observed that low spin state is more prominent in the flat geometry of graphene.[48] The doping concentration of Mn and the synthesis condition (like oxygen environment) of the graphene oxide sample is optimized to stabilize Mn^{2+} oxygen state. The covalently bonded oxygen atom in one of the sub-lattice of GO and Mn ion generate the magnetic moment in GO cluster. The doping of Mn restores damaged C conjugation and removes some OH and COOH group through long range C-O-Mn bonding for long range magnetic ordering. The exchange interaction between the clusters have notable impact on the magnetic moment of doped GO system at low energy difference and nano range.[49] Fig. 7 displays the isothermal magnetization data measured on MnGO10 composite at 77, 150, 300, 350 and 400 K with the magnetic field varied from -2 kOe to +2kOe. A clear, s-shape saturated open hysteresis loops (M (H) curve) were observed at all the different temperatures measured including at 300 K, within the range of magnetization from ~ 0.024 to ~0.018 emu/g. It can be noticed that at lower temperature, magnetic moment enhanced as compared to room temperature as well as at higher temperature. Because, at higher temperature, the phonon scattering destroys the net magnetic moment of free and Mn-bonded graphene lattice.

4. Conclusions

In summary, luminomagnetic bifunctionality of Mn^{2+}-bonded graphene oxide/reduced graphene oxide two dimensional nanosheets offers a new paradigm shift in the engineering of graphene analogs for tuning optical and magnetic properties. The manganese oxide nanoparticles are distributed over the wrinkled GO/RGO nanosheets. Ultraviolet-visible absorption spectroscopy results convincingly show the intercalation and adsorption of Mn^{2+} ions onto the GO/RGO sheets. The photoluminescence (PL) spectra excited by different wavelengths are revealed that the

resonant energy transfer between Mn^{2+} and sp^3/sp^2 clusters of GO/RGO is responsible for the enhancement of broad range of wavelengths emission. This enhanced tunable PL is strongly related to the induced changes of its heterogeneous electronic structures and bonding properties. The weak longer wavelength emission is observed in Mn^{2+} bonded RGO as compared to Mn^{2+} bonded GO composite due to the hopping and tunneling effects which facilitated the migration of excitons to nonradiative recombination sites. Moreover, the complex pH-sensitive PL behaviors have also been examined. The ferromagnetic behavior occurs from the defects on Mn^{2+} bonded GO composite. We visualize that such accomplishments will be key to developing the much-awaited high performance applications of graphene and its analogs in the fields of various technological applications.

Notes and references

[a]*CSIR - National Physical Laboratory, Dr K S Krishnan Road, New Delhi, 110012, India*
[b]*Department of Physics, Kalindi College, University of Delhi, New Delhi, 110008, India*
[c]*Energy Material and Devices Laboratory, Department of Physics, RTM Nagpur University, Nagpur, 440033, India*
[d]*Department of Chemistry, Pittsburg State University, Pittsburg, KS, 66762, USA*
[e]*CSIR-Advanced Materials and Processes Research Institute, Bhopal, 462024, India*
†*Both authors are equally contributed.*

* *Corresponding author. Tel.: +91-11-45609385, Fx: +91-11-45609310*
E-mail address: **bipinbhu@yahoo.com**

† Electronic Supplementary Information (ESI) available: [details of any supplementary information available should be included here]. See DOI: 10.1039/b000000x/

‡ Footnotes should appear here. These might include comments relevant to but not central to the matter under discussion, limited experimental and spectral data, and crystallographic data.

Acknowledgment

The authors wish to thank Director, N.P.L., New Delhi for his keen interest in the work. The authors are thankful to Prof. O.N. Srivastava (Banaras Hindu University, Varanasi) for his encouragement. The authors gratefully acknowledged University Grant Commission (UGC) and Council of Scientific and Industrial Research (CSIR), Govt.of India for financial assistance to carry out this work.

References:

(1) P. V. Kamat, *J. Phys. Chem. Lett.* 2011, **2**, 242-251.
(2) C. H. Chuang, Y. F. Wang, Y. C. Shao, Y. C. Yeh, D. Y. Wang, C. W. Chen, J. W. Chiou, S. C. Ray, W. F. Pong, L. Zhang, J. F. Zhu and J. H. Guo, *Sci. Rep.* 2014, **4**, 4525.
(3) H. Yamaguchi, G. Eda, C. Mattevi, H. Kim and M. Chhowalla, *ACS Nano* 2010, **4**, 524-528.
(4) C. T. Chien, S. S. Li, W. J. Lai, Y. C. Yeh, H. A. Chen, I. S. Chen, L. C. Chen, K. H. Chen, T. Nemoto, S. Isoda, M. Chen, T. Fujita, G. Eda, H. Yamaguchi, M. Chhowalla, C. W. Chen, *Angew. Chem. Int. Ed.* 2012, **51**, 6662-6666.
(5) S. Gilje, S. Han, M. Wang, K. L. Wang and R. B. Kaner, *Nano Lett.* 2007, **7**, 3394-3398.
(6) J. L. Li, H. C. Bao, X. L. Hou, L. Sun, X. G. Wang and M. Gu, *Angew. Chem. Int. Ed.* 2012, **51**, 1830-1834.
(7) R. J. W. E. Lahaye, H. K. Jeong, C. Y. Park and Y. H. Lee, *Phys. Rev. B.* 2009, **79**, 125435.
(8) S. Saxena, T. A. Tyson and E. Negusset, *J. Phys. Chem. Lett.* 2010, **1**, 3433-3437.
(9) Z. Luo, P. M. Vora, E. J. Mele, A. T. C. Johnson and J. M. Kikkawa, *Appl. Phys. Lett.* 2009, **94**, 111909.
(10) C. Galande, A. D. Mohite, A. V. Naumov, W. Gao, L. Ci, A. Ajayan, H. Guo, A. Srivastava, R. B. Weisman and P. M. Ajayan, *Sci. Rep.* 2011, **1**, 85.
(11) J. L. Chen, and X. P. Yan, *Chem. Commun.* 2011, **47**, 3135-3137.
(12) J. I. Paredes, S. Villar-Rodil, A. Mart´Inez-Alonso and J. M. D. Tasc´On, *Langmuir* 2008, **24**, 10560-10564.
(13) Z. Gan, S. Xiong, X. Wu, T. Xu, X. Zhu, X. Gan, J. Guo, J. Shen, L. Sun and P. K. Chu, *Adv. Opt. Mater.* 2013, **1**, DOI: 10.1002/adom.201300368.
(14) K. P. Loh, Q. Bao, G. Eda and M. Chhowalla, *Nature Chem.* 2010, **2**, 1015-1024.
(15) T. Gokus, R. R. Nair, A. Bonetti, M. Bohmler, A. Lombardo, K. S. Novoselov, A. K. Geim, A. C. Ferrari and A. Hartschuh, *ACS Nano* 2009, **3**, 3963-3968.
(16) Z. Luo, P. M. Vora, E. J. Mele, A. T. C. Johnson, J. M. Kikkawa, *Appl. Phys. Lett.* 2009, **94**, 111909.
(17) G. Eda, Y. Y. Lin, C. Mattevi, H. Yamaguchi, H. A. Chen, I. S. Chen, C. W. Chen and M. Chhowalla, *Adv. Mater.* 2010, **22**, 505-509.
(18) D. Y. Pan, J. C. Zhang, Z. Li, M. H. Wu, *Adv. Mater.* 2010, **22**,734-738.
(19) J. Du, X. Y. Lai, N. L. Yang, J. Zhai, D. Kisailus, F. B. Su, D. Wang, L. Jiang, *ACS Nano* 2011, **5**, 590-596.
(20) Y. Y. Liang, Y. G. Li, H. L. Wang, J. G. Zhou, J. Wang, T. Z. Regier, H. J. Regier, *Nat. Mater.* 2011, **10**, 780-786.
(21) Z. S. Wu, W. C. Ren, D. W. Wang, F. Li, B. L. Liu and H. M. Cheng, *ACS Nano* 2010, **10**, 5835-5842.
(22) Q. S. Mei, K. Zhang, G. J. Guan, B. H. Liu, S. H. Wang and Z. P. Zhang, *Chem. Commun.* 2010, **46**, 7319-7321.
(23) Z. X. Gan, S. J. Xiong, X. L. Wu, C. Y. He, J. C. Shen and P. K. Chu, *Nano Lett.* 2011, **11**, 3951-3956.
(24) H. Li, H. He, T. Zhang, L. Sun and Z. Ye, *RSC Adv.* 2014, **4**, 54832-54836.
(25) X. Yang, H. Xia, X. Qin, W. Li, Y. Dai, X. Liu, M. Zhao, Y. Xia, S. Wang and B. Yan, *Carbon* 2009, **47**, 1399-1406.
(26) K. S. Novoselov, A. K. Geim, S. V. Morozov, D. Jiang, Y. Zhang, S. V. Dubonos, I. V. Grigorieva and A. A. Firsov, *Science* 2004, **306**, 666-669.
(27) L. Li, R. Qin, H. Li, L. Yu, Q. Liu, G. Luo, Z. Gao and J. Gao *ACS Nano* 2011, **5**, 2601-2610.
(28) R. McIntosh, M. A. Mamo, B. Jamieson, S. Roy and S. Bhattacharyya, *Euro phys. Lett.* 2012, **97**, 38001.
(29) Y. Wang, Y. Huang, Y. Song, X. Zhang, Y. Ma, J. Liang and Y. Chen, *Nano Lett.* 2009, **9**, 220-224.
(30) H. S. S. Ramakrishna Matte, K. S. Subrahmanyam, C. N. R. Rao, *J. Phys. Chem. Lett.* 2009, **113**, 9982-9985.
(31) J. Barzola-Quiquia, R. Hohne, M. Rothermel, A. Setzer, P. Esquinazi and V. Heera, *Eur. Phys. J. B* 2008, **61**, 127-130.
(32) W. S. Hummers and R. E. Offeman, *J. Am. Chem. Soc.*1958, **80**, 1339-1339.
(33) B. K. Gupta, P. Thanikaivelan, T. N. Narayanan, L. Song, W. Gao, T. Hayashi, A. L. M. Reddy, A. Saha, V. Shanker, M. Endo, A. A. Marti and P. M. Ajayan, *Nano letters*, 2011, **11**, 5227-5233.
(34) Y. Gan, L. Sun and F. Banhart, *Small*, 2008, **4**, 587-591.
(35) G. Kedawat, S. Srivastava, V. K. Jain, P. Kumar, V. Kataria, Agrawal, Y. B. K. Gupta and Y. K. Vijay, *ACS Appl. Mater. Interfaces* 2013, **5**, 4872-4877.
(36) B. K. Gupta, D. Haranath, S. Saini, V. N. Singh and V. Shanker, *Nanotechnol.* 2010, **21**, 055607.

(37) X. Tong, H. Wang, G. Wang, L. Wan, Z.Ren and J. J. Bai, *Solid State Chem.* 2011, **184**, 982-989.
(38) W. Gao, L. B. Alemany, L. Ci and P. M. Ajayan, *Nat. Chem.* 2009, **1**, 403-408.
(39) K. N. Kudin, B. Ozbas, H. C. Schniepp, R. K. Prud'homme, I. A. Aksay and R. Car, *Nano Lett.* 2008, **8**, 36-41.
(40) Ferrari, A. C. *Solid State Commun.* 2007, **143**, 47-57.
(41) Y. Y. Wang, Z. H. Ni, T. Yu, Z. X. Shen and H. M. Wang, *J. Phys. Chem. C* 2008, **112**, 10637-10640.
(42) J. Gao, F. Liu, Y. Liu, N. Ma, Z. Wang and X. Zhang, *Chem. Mater.* 2010, **22**, 2213-2218.
(43) A. C. Ferrari, J. C. Meyer, V. Scardaci and C. Casiraghi, *Phys. Rev. Lett.* 2006, **97**, 187401.
(44) Z. Ai, L. Zhang, F. Kong, H. Liu, W. Xing and J. Qiu, *Mater. Chem. Phys.* 2008, **111**, 162-167.
(45) J. Dwivedi, P. Kumar, A. Kumar, Sudama, V. N. Singh, B. P. Singh, S. K. Dhawan, V. Shanker and B. K. Gupta, *RSC Advances*, 2014, **4**, 54936-54947.
(46) B. K. Gupta, T. N. Narayanan, S. A. Vithayathil, Y.Lee, S. Koshy, A. L. M. Reddy, A.Saha, V. Shanker, V. N. Singh, B. A. Kaipparettu, A. A. Martí and P. M. Ajayan, *Small*, 2012, **8**, 3028-3034.
(47) B. K. Gupta, V. Rathee, T. N. Narayanan, P. Thanikaivelan, A. Saha, Govind, S. P. Singh, V. Shanker, A. A. Marti and P. M. Ajayan, *Small*, 2011, **7**, 1767-1773.
(48) M. Sepioni, S. Rablen, R. R. Nair, J. Narayanan, F. Tuna, R. Winpenny, A. K. Geim and I. V. Grigorieva, *Phys. Rev. Lett.* 2010, **105**, 207205.
(49) D. W. Boukhvalov and M. I. Katsnelson, *ACS Nano* 2011, **5**, 2440-2446.

†Electronic Supplementary Information (ESI)

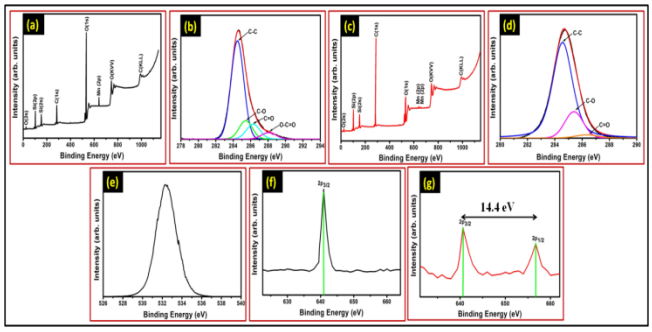

Fig. S1: (a) XPS spectrum of MnGO10 composite, (b) high resolution spectra of C1s region for MnGO10 composite, (c) XPS spectrum of MnRGO10 composite, (d) high resolution spectra of C1s region for MnRGO10 composite, (e) core level peak of O1s for MnGO10 composite, (f) high resolution core level peak of Mn2p for MnGO10 composite and (g) high resolution core level peak of Mn2p for MnRGO10 composite

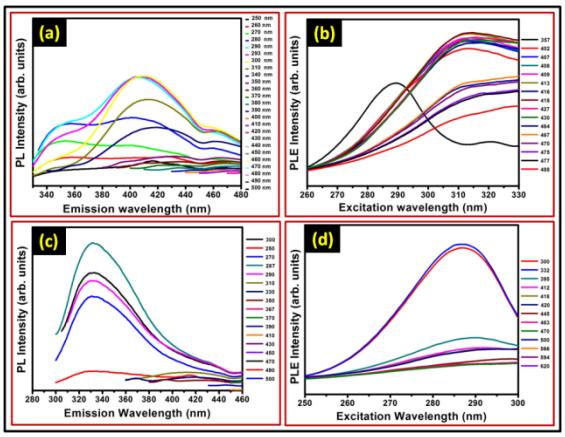

Fig. S2: PL emission spectra for MnGO10 composite, (b) PLE spectra for MnGO10 composite at different monitoring and excitation wavelengths, respectively, (c) PL emission spectra for MnRGO10 composite and (d) PLE spectra for MnRGO10 composite at different monitoring and excitation wavelengths, respectively.

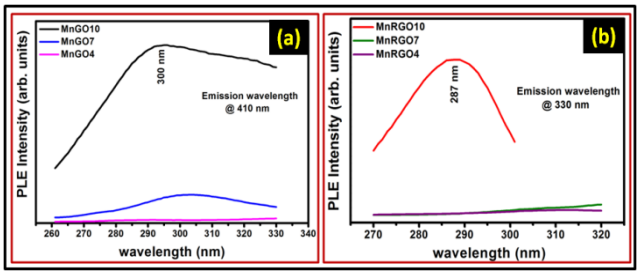

Fig. S3: PLE spectra for (a) MnGO and (b) MnRGO composite at different pH values (4, 7 and 10).

Graphical Table of Contents (TOC)

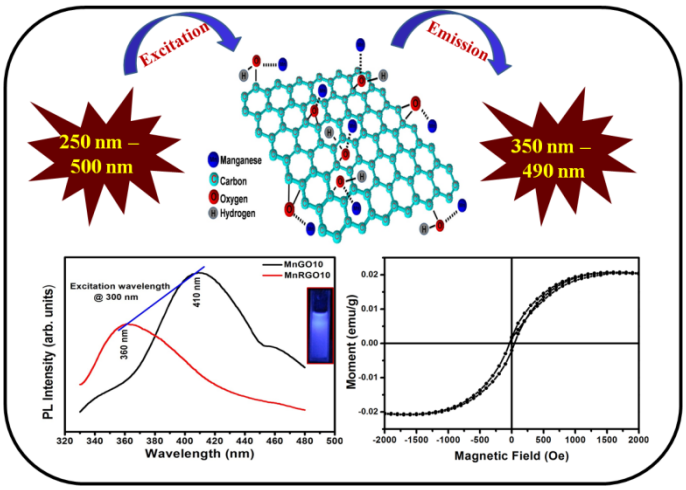

Demonstration of luminomagnetic two-dimensional Mn^{2+} bonded graphene oxide/reduced graphene oxide nanosheets synthesized by solvothermal reduction method for various technological applications.